# Eddy Current Loss Reduction in Binder Jet Printed Iron Silicon Cores

Bhuvan Khoshoo, *Student Member, IEEE*, Khan Jazib Islam, Hawke Suen, Patrick Kwon, Jorge Peña Lozano, and Shanelle N. Foster, *Senior Member, IEEE*

2022 International Conference on Electrical Machines (ICEM) | 978-1-6654-1432-6/22/$31.00 ©2022 IEEE | DOI: 10.1109/ICEM51905.2022.9910749

***Abstract*—Additive manufacturing of soft magnetic iron cores can help realize electric machines with increased power density. However, high eddy current loss in the 3D printed bulk iron core is a big challenge before AM can be used for commercial production of electric machines. This article discusses a method to reduce the specific loss density of 3D printed iron cores using binder jet printing. It is shown that reducing the size of boron particle, used as a sintering aid, results in lower core loss without significant change in magnetization of the sample. Extracted material properties of presented samples are further validated by finite element simulations using a permanent magnet machine. Performance comparison in the entire torque/speed envelop shows eddy current loss reduction and efficiency improvement in the flux weakening region.**

***Index Terms*—Additive manufacturing, 3D printing, binder jet printing, electric machines, printed iron silicon, hysteresis loss, eddy current loss, finite element analysis, torque/speed envelop.**

## I. Introduction

In the last decade, consistent efforts have been made to improve and advance the design of electric machines and simultaneously electric/hybrid electric vehicles (EVs/HEVs) to address the environmental challenges [1]–[3]. Although personal vehicles with electrification are available to consumers, there is a huge demand to increase the power density and reliability of electric machines to reach even higher speeds. According to the U.S. Department of Energy (DOE), the Electrical and Electronics Technical Team (EETT) has a 2025 power density research target of 50 kW/L for electric motors [4]. Currently, motors employed in even the best EVs/HEVs present in the market are nowhere close to the proposed power density values [5]. Additionally, faults in electric machines can lead to adverse conditions in the machine performance and may be dangerous to human safety [6]–[8]. Therefore, additional focus is required to address the reliability issues, which may be solved by employing unique machine designs with high fault tolerance [9]. It is therefore essential to think beyond the limitations of conventional manufacturing technologies to achieve these ambitious targets.

Additive manufacturing (AM) can open pathways to the next generation electric machines. With AM, it is possible to manufacture unprecedented designs of unusual shapes and material combinations, which is not possible with conventional technology. In electric machines, the application of AM in printing soft magnetic materials is of particular interest since iron cores are responsible for guiding the magnetic flux and also make up the bulk volume of the machine. Traditionally, iron cores are made of electrical steel laminations stacked together, which are typically made from Fe-Si, Fe-Ni, or Fe-Co alloy and provide good magnetic and mechanical properties, such as high permeability, high saturation, low iron losses, and high tensile and yield strength [10], [11]. Out of the three alloys mentioned, Fe-Si is prominently used in the design of transformers and electric machines and remains the focus of AM research due to its superior electrical resistivity, relatively simple processability, and performance per cost [12], [13].

AM gives freedom to explore designs beyond the current limitations; however, there are still challenges associated with the performance of 3D printed Fe-Si cores. 3D printed bulk iron cores have high iron loss, especially eddy current loss, which reduces efficiency compared to their conventional counterparts. Although examples of 3D printed iron cores used to build electric machines can be found in literature [14]–[20], very few of these studies analyze the loss (and efficiency) performance of such machines. In [19], authors printed the rotor core of a switched reluctance motor (SRM) using high silicon content material and compared its performance with the conventional SRM. While the two machines have comparable performance at base speed (600 RPM), the 3D printed SRM shows almost 18% lower efficiency at 2.5 times the base speed due to increased eddy current loss in the solid rotor core. Magnetic properties of commercially available Fe-Si varnished steel (M300-35A) and AM material, Fe-36%Ni powder (INVAR 36), were compared in [20]. The printed material had 17 times higher losses at 50 Hz and magnetic polarization of 1 T.

Clearly, it is imperative to address the issue of high iron loss before AM material can be used commercially to manufacture electric machines. Several strategies such as improving the chemical composition of the AM material by increasing Si content in the Fe-Si alloy and printing intermetallic or air-gap layers between soft magnetic layers

This work was partially supported in part by the Department of Navy, Office of Naval Research for sponsoring this work, under ONR Award Number N00014-18-1-2514. This material is also based upon work supported by the National Science Foundation under Grant No. 2045776.

Bhuvan Khoshoo, Khan J. Islam, Jorge P. Lozano, and Shanelle N. Foster are with Department of Electrical and Computer Engineering, Michigan State University, East Lansing, MI 48824 USA (e-mail: khoshoob@msu.edu; islamkha@msu.edu; penaloz2@msu.edu; hogansha@egr.msu.edu).

Hawke Suen and Patrick Kwon are with the Department of Mechanical Engineering, Michigan State University, East Lansing, MI 48824 USA (e-mail: hoihohaw@msu.edu; pkwon@egr.msu.edu).

have been explored to tackle this issue [21], [22]. However, increasing the Si content makes the resulting alloy highly brittle, which will restrict the application of AM in printing rotor core for application at high speeds. On the other hand, although introducing air-gap or intermetallic layers will reduce the eddy current loss by dividing the core into virtual segments, it will also reduce the material's filling factor leading to lower air-gap flux density and average torque. It was shown that the use of boron particles for manufacturing Fe-Si using binder jet printing (BJP) results in an increase in relative permeability, reduction of hysteresis losses, and increased grain size, and thus has the potential for usage in low speed applications [23]. However, the study did not include the impact of changing boron particle size on the material's magnetic properties.

This work then analyzes the improvement in magnetic characteristics of 3D printed Fe-Si due to variation in boron particle size. It also makes an attempt to verify that the relative improvement in material properties is reflected in actual machine performance over the entire torque/speed range through 2D finite element analysis (FEA).

The rest of the paper is structured as follows: Section II discusses the background of using boron in Fe-Si and sample preparation for characterization. Section III highlights the impact of boron particle size on the magnetic properties of Fe-Si manufactured using BJP by discussing experimental results. Section IV discusses the electric machine details and FEA setup used in this work. Section V presents the FEA results and the proposed method's impact on machine performance. Finally, the study is concluded in Section VI.

## II. Background and Sample Preparation

Relative density of 3D printed metallic green parts manufactured using a powder bed method like BJP can only reach about 50-60% of the theoretical density. It was shown that using boron as a sintering aid helps increase the relative density of 3D printed sample [24]. The addition of boron also affects the grain size and boundary, ultimately impacting the magnetic properties such as specific loss density [25]. During magnetization, the grain boundaries restrict the domain movement by acting as barriers, which helps decrease the losses. However, there is an optimum grain size for the best loss reduction. While larger grain size results in lower hysteresis loss [23], it increases the domain size and the eddy current loss.

### A. Sample Preparation

Although the impact of using boron as an additive has been studied previously, the impact of controlling boron particle size on magnetic properties has not been explored yet. It is known that the particle size influences diffusion and segregation, thereby, the grain boundary characteristics. Therefore, in this work, the impact of changing boron particle size on the magnetic properties of 3D printed Fe-Si is studied. For this purpose, three toroidal ring samples are printed

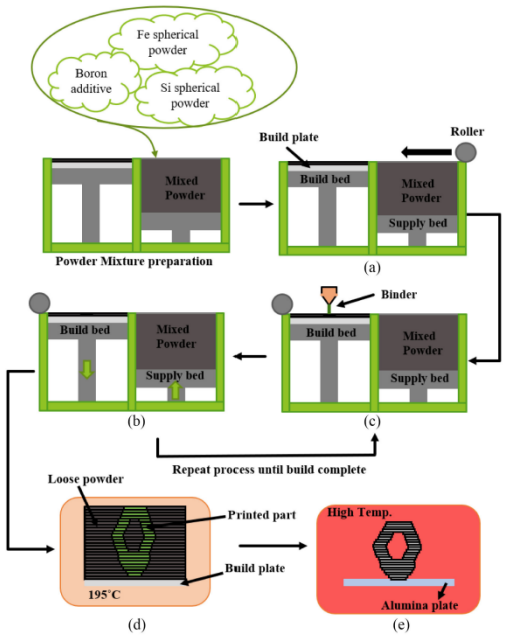


Fig. 1. Schematic of BJP process [23].

TABLE I
Summary of BJP samples used for magnetic characterization.

| Parameters | Sample 1 | Sample 2 | Sample 3 |
|---|---|---|---|
| Sample Composition | $Fe_{95}Si_5$ | $Fe_{95}Si_5$ | $Fe_{95}Si_5$ |
| Sintering Temperature | 1200°C | 1200°C | 1200°C |
| Boron Content | 0.25% | 0.25% | 0.25% |
| Boron Particle Size | 0.1$\mu$m | 0.5$\mu$m | 1.0$\mu$m |

using the BJP process illustrated in Fig. 1 [23]. The ring samples have an outer diameter of 32.5 mm, inner diameter of 25.4 mm, and height of 3.5 mm. For a fair comparison, the boron content is identical in all three samples.

For powder stock preparation, $FeSi_8$ spherical alloyed powder (-45+15$\mu$m) from Carpenter Additive is mixed with 33wt% of smaller pure iron powder ($< 10\mu$m) from Sigma-Aldrich to reduce the silicon content and increase powder packing. The ratio is calculated with the linear packing model developed by Stovall et al. [26]. Then the powder is added with the desired amount of boron and mixed with a high-speed mixer (FlackTek Inc. SC, USA) at 1500 RPM for 100 seconds. The powder is then processed by a Binder Jetting 3D printer manufactured by ExOne (PA, USA) with a 2.1 powder feed ratio. The binder saturation rate is 70%, assuming the powder packing is 60% dense. After the sample is printed, the part is placed in an air furnace for binder curing at 195°C for 2 hours. At last, the cured samples are placed into an environment-controlled resistance furnace (Materials Research Furnaces, NH, USA) and sintered at 1200°C in a 120.8 kPa argon atmosphere for 6 hours. For less oxygen content, the furnace chamber is pumped down to 1.33 Pa and purged with argon three times. The sample compositions and boron particle sizes used for the samples are given in Table I.

### B. Magnetic Characterization

Magnetic characterization is performed using a commercially available soft magnetic testing apparatus (Magnetic Instrumentation, USA). Standards ASTM A773 [27] and ASTM A927 [28] are used to perform dc and ac characterizations, respectively. For both dc and ac characterizations, three separate measurements are taken at each level and averaged to arrive at the final values. For dc characterization, quasi-static testing is done at an excitation frequency of 1 Hz. Magnetic properties extracted via dc characterization include maximum relative permeability $\mu_{r,max}$, intrinsic coercivity $H_c$, and magnetic flux density $B_5$, $B_{25}$, and $B_{100}$ at 500 A/m, 2500 A/m, and 10,000 A/m respectively. Hysteresis loss per cycle ($P_h/f$) is calculated from the area enclosed within the quasi-static B-H curve. For ac characterization, specific loss density curves at excitation frequencies of 50 Hz, 200 Hz, and 400 Hz are extracted at three magnetic flux density levels, 0.5 T, 1.0 T, and 1.5 T.

## III. Experimentally Extracted Magnetic Properties

Experimental results show that while reducing the boron particle size does not impact the maximum relative permeability, $\mu_{r,max}$, it slightly improves the magnetic induction of the material, such as $B_5$, $B_{25}$, and $B_{100}$, as shown in Table II. It is also observed that reducing the boron particle size has a nonlinear impact on the intrinsic coercivity, with Sample 3 showing the lowest $H_c$ while Sample 2 showing the highest $H_c$, as shown in Fig. 2 and Table II. As expected, hysteresis loss per cycle, $P_h/f$, also changes corresponding to $H_c$, as shown in Table II.

For the three materials, the specific loss density trend is reversed, with Sample 3 showing the highest specific loss at all magnetic flux density levels and frequencies, as shown in Fig. 3. While reducing boron particle size leads to decreased core losses in general, it is worth mentioning that the impact is not linear. Sample 1 with boron particle size 0.1$\mu$m shows the lowest loss density at low magnetic saturation levels. However, with an increase in magnetic flux density, Sample 2 with boron particle size 0.5$\mu$m performs the best. These preliminary results indicate that the relationship between boron particle size and the magnetic properties of Fe-Si alloy is somewhat complex, and further analysis is required to achieve optimal boron particle size. Nevertheless, it is possible to decrease core losses by almost 10% without significant change in material magnetization, as seen from experimental results. This improvement in core losses shows potential for using 3D printed iron cores manufactured by BJP in high-speed applications.

## IV. Finite Element Setup

The performance of BJP samples with different boron particle sizes is further evaluated by 2D FEA using a 48-slot/8-pole interior permanent magnet (IPM) machine [29]. Some critical parameters of the chosen machine are given

TABLE II
Experimental Results From DC Characterization.

| Extracted Properties | Sample 1 | Sample 2 | Sample 3 |
|---|---|---|---|
| $\mu_{r,max}$ | 4819.61 | 4658.51 | 4751.25 |
| $H_c$ (A/m) | 55.23 | 58.53 | 45.14 |
| $B_5$ (T) | 1.11 | 1.1 | 1.08 |
| $B_{25}$ (T) | 1.34 | 1.35 | 1.32 |
| $B_{100}$ (T) | 1.63 | 1.62 | 1.57 |
| $P_h/f$ (Ws/kg) | 0.068 | 0.079 | 0.048 |

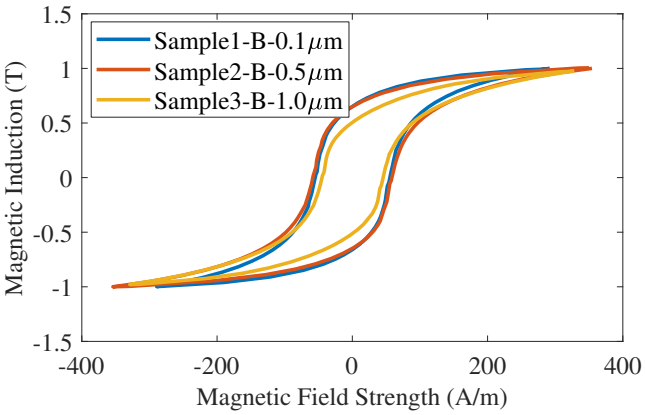


(a) $B_{max}$ = 1 T.

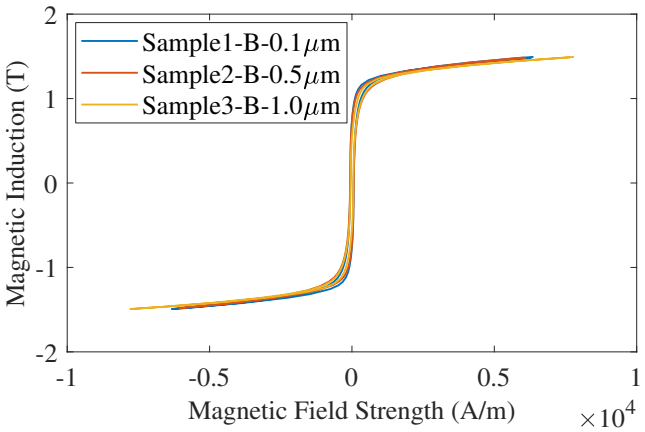


(b) $B_{max}$ = 1.5 T.

Fig. 2. Quasi-static hysteresis loops of BJP samples at different magnetic flux density levels.

in Table III, and a 2D model of the machine is shown in Fig. 4. For a fair comparison, the machine's basic dimensions and winding configuration are kept unchanged, and only the material used to define the rotor and stator iron core is changed. Based on the extracted material properties in the previous section, three cases are defined for analysis:

- Case 1 – $Fe_{95}Si_5$ with boron particle size 0.1$\mu$m,
- Case 2 – $Fe_{95}Si_5$ with boron particle size 0.5$\mu$m,
- Case 3 – $Fe_{95}Si_5$ with boron particle size 1.0$\mu$m.

All cases are compared at various operating conditions, covering the entire torque/speed envelop, using the JMAG-Designer software tool [30]. The three materials are defined

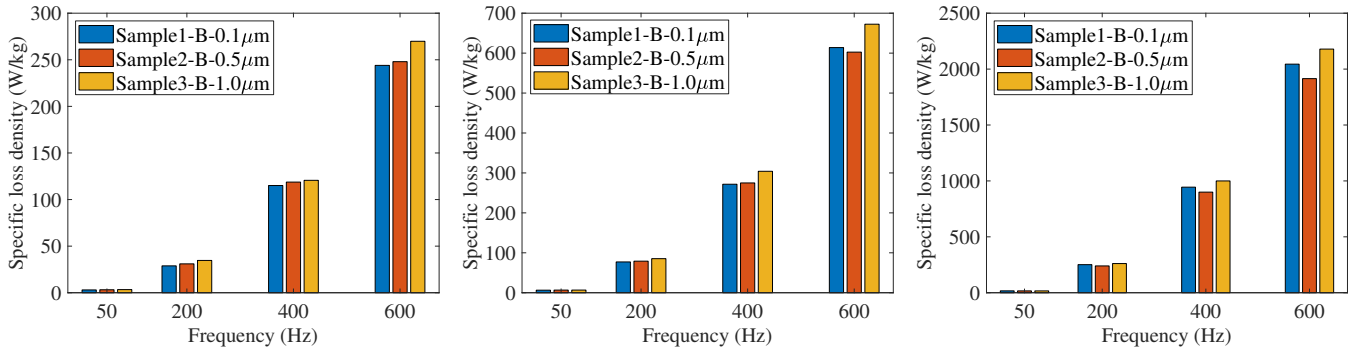


(a) B = 0.75 T. (b) B = 1 T. (c) B = 1.5 T.

Fig. 3. Core loss density at different induction levels for the three samples with different boron particle size.

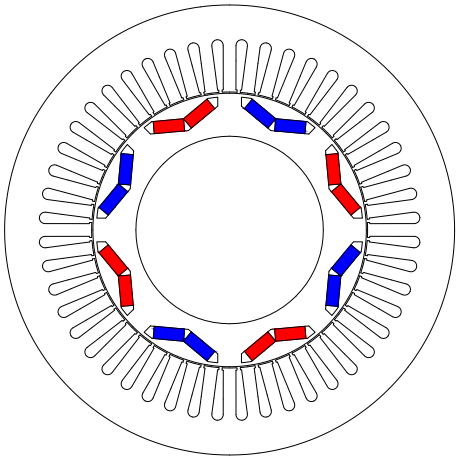

Fig. 4. 2D model of IPM machine used for analysis.

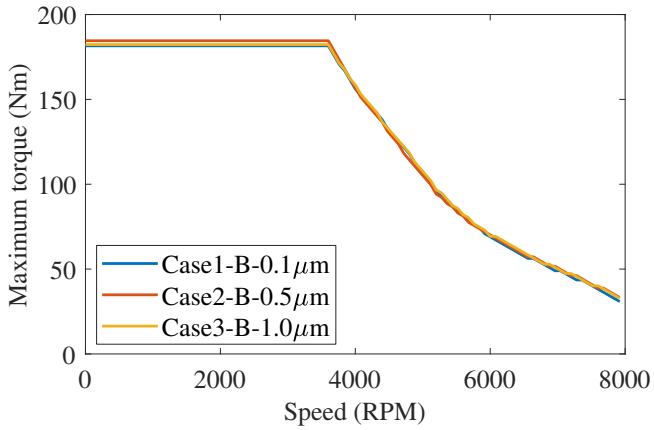


Fig. 5. Torque/speed profile of the three simulated cases.

TABLE III
PARAMETERS OF IPM MACHINE USED FOR ANALYSIS.

| Parameters | Values | Parameters | Values |
|---|---|---|---|
| Mechanical power | 69 kW | Turns per coil | 11 |
| Rated speed | 3000 RPM | Slot/pole/phase | 2 |
| Peak current | 177 A | Slot fill factor | 0.46 |
| Stator outer diameter | 264 mm | Air-gap | 0.75 mm |
| Rotor outer diameter | 160.4 mm | Stack length | 50.8 mm |
| Magnet type | NdFeB | DC-link voltage | 650 V |

using their experimentally extracted B-H curves and specific loss density curves at different frequencies. Maximum speed is defined as 8000 RPM, and the maximum excitation current is limited to 177 A. For all cases, a dc-link voltage of 650 V is used as the voltage limit. The iron loss is calculated in JMAG using the Preset 1 method from the experimentally extracted loss data [31].

## V. FINITE ELEMENT RESULTS

For all cases, machine performances are computed considering maximum torque per ampere (MTPA) control until base speed and flux weakening control beyond base speed. It is observed that all three cases have a similar torque/speed profile, as shown in Fig. 5. Additionally, all three cases have similar base speeds, close to 3600 RPM.

Analysis of loss profiles of the three cases shows that both Cases 1 and 2 have higher hysteresis loss in the entire speed range than Case 3, with Case 2 showing the highest loss values as shown in Fig. 6. However, Case 1 with boron particle size 0.1$\mu$m has the lowest eddy current losses out of the three, in almost the entire speed range, as shown in Fig. 7. Moreover, since eddy current losses make up most of the iron loss in iron cores, a similar trend is observed in the total iron loss profiles of the three cases. Further evaluation at operating points corresponding to maximum torque shows the highest iron loss values in the entire speed range for Case 3. In fact, Case 1 shows almost 11% lower iron loss compared to Case 3 at speeds greater than 4000 RPM, as shown in Fig 8. This decrease in the iron loss for Case 1 ultimately translates to increased efficiency, especially in the flux weakening region.

A summary of electromagnetic torque, mechanical power, hysteresis loss, eddy current loss, and efficiency at operating points corresponding to maximum torque at 3600 RPM (base speed) and 7200 RPM are given in Table IV. Interestingly, Case 1 with boron particle size 0.1 $\mu$m has the lowest eddy current loss (and iron loss) and the highest efficiency

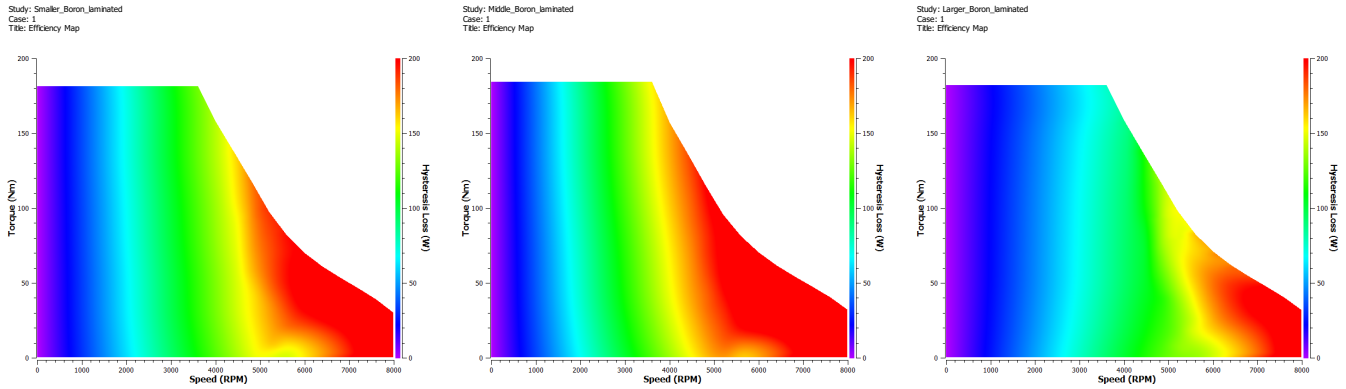


(a) Case 1 with boron particle size = 0.1 $\mu$m. (b) Case 2 with boron particle size = 0.5 $\mu$m. (c) Case 3 with boron particle size = 1.0 $\mu$m.

Fig. 6. Combined hysteresis loss profile (stator and rotor) of three simulated cases.

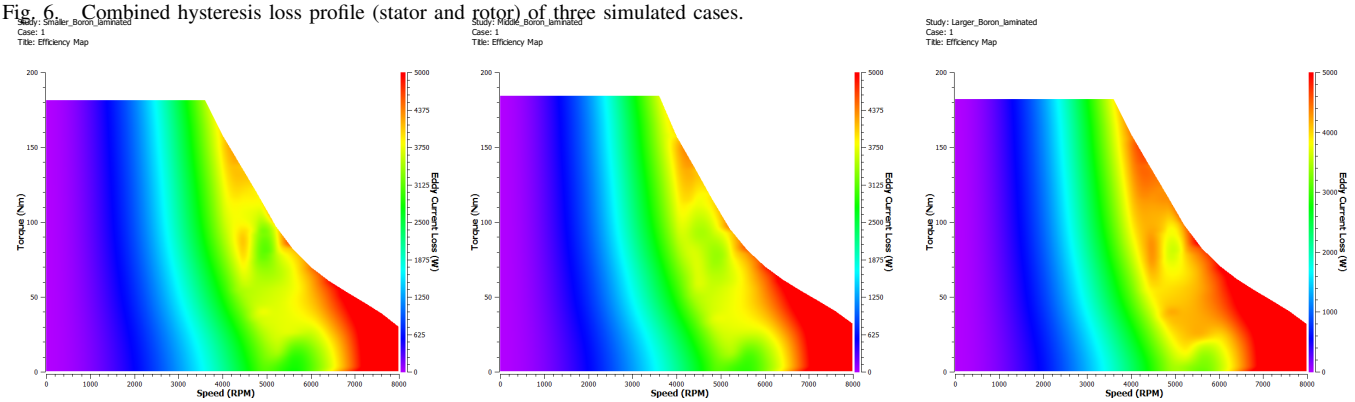


(a) Case 1 with boron particle size = 0.1 $\mu$m. (b) Case 2 with boron particle size = 0.5 $\mu$m. (c) Case 3 with boron particle size = 1.0 $\mu$m.

Fig. 7. Combined eddy current loss profile (stator and rotor) of three simulated cases.

TABLE IV
FEA RESULTS AT OPERATING POINT CORRESPONDING TO MAXIMUM TORQUE AT 3600 RPM AND AT 7200 RPM FOR THE SIMULATED CASES.

| Performance Measure | Speed = 3600 RPM | | | Speed = 7200 RPM | | |
|---|---|---|---|---|---|---|
| | Case 1 | Case 2 | Case 3 | Case 1 | Case 2 | Case 3 |
| Electromagnetic Torque (Nm) | 181.58 | **184.55** | 182.28 | 45.39 | 46.14 | **47.39** |
| Output Power (kW) | 68.45 | **69.57** | 68.71 | 34.22 | 34.78 | **35.73** |
| Hysteresis loss (W) | 129.00 | 154.90 | **76.52** | 226.35 | 258.08 | **199.19** |
| Eddy Current loss (W) | **3495.14** | 3688.18 | 3861.21 | **5862.89** | 6261.51 | 6648.13 |
| Efficiency (%) | **89.78** | 89.67 | 89.44 | **82.88** | 82.26 | 81.93 |

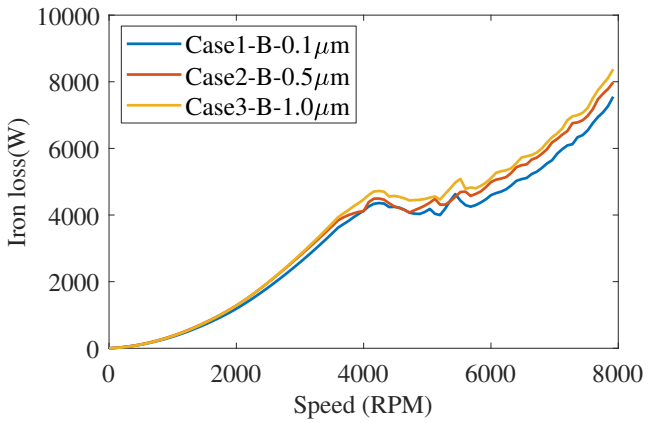


Fig. 8. Iron loss of simulated cases at operating points corresponding to maximum torque in entire speed range.

at both operating points. Machine operation beyond base speed requires suppression of magnet flux to maintain the limit imposed by dc-link voltage. A comparison of the magnetic flux density plots for Case 1 corresponding to the two operating points discussed in Table IV shows that the magnetic flux density in the stator decreases with an increase in speed (see Fig. 9). In fact, flux density in most of the stator core at 7200 RPM is below 0.75 T, as shown in Fig. 9(b). This decrease in magnetic flux density becomes more dominant as the rotational speed increases. Consequently, Case 1 with boron particle size 0.1$\mu$m shows the lowest iron loss in the flux weakening region due to its superior loss properties at lower flux density values. Moreover, Case 1 shows almost 1% higher efficiency than Case 3 at 7200 RPM, as shown in Table IV.

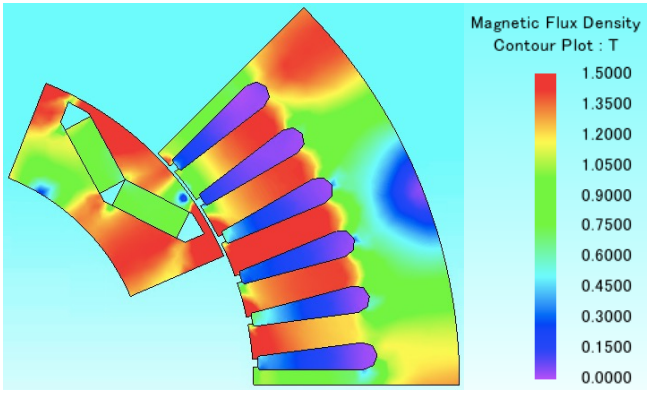


(a)

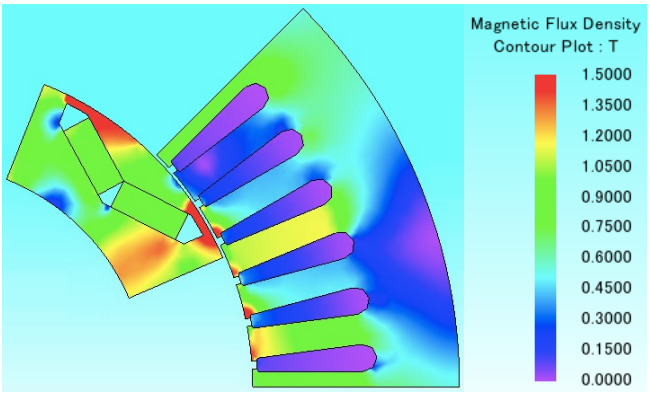


(b)

Fig. 9. Magnetic flux density plots at operating point corresponding to maximum torque for Case 1 at (a) 3600 RPM and (b) 7200 RPM.

## VI. Conclusion

Variation in boron particle size used as the sintering aid for manufacturing Fe-Si using binder jet printing (BJP) can lead to improved specific loss properties without any significant change in magnetization of the material. Experimental characterization of three Fe-Si samples with three different boron particle sizes has shown that the relation between boron particle size and magnetic properties is nonlinear and somewhat complex. Nevertheless, a reduction in core losses by almost 10% without a significant change in magnetization properties has been demonstrated.

Magnetic properties of the three materials have been further validated utilizing 2D finite element simulation results of a 48-slot/8-pole IPM machine over the entire torque/speed range. Reducing the boron particle size leads to more than 10% decrease in iron loss and almost 1% increase in efficiency in the flux weakening region. Future work shall include further investigation of the impact of boron particle size variation on the material's magnetic properties. 3D printed Fe-Si alloy manufactured using BJP may have further potential of reduction in iron loss with the help of optimal material deposition in iron cores.

## References

[1] "Commission Regulation (EU) 2019/1781 of 1 October 2019," https://op.europa.eu/en/publication-detail/-/publication/218c6599-f734-11e9-8c1f-01aa75ed71a1/language-en/.

[2] "Energy Department Awards $22 Million to Support Next Generation Electric Machines for Manufacturing," https://www.energy.gov/articles/energy-department-awards-22-million-support-next-generation-electric-machines-manufacturing/.

[3] A. Aggarwal, E. G. Strangas, and A. Karlis, "Review of segmented stator and rotor designs for ac electric machines," in *2020 International Conference on Electrical Machines (ICEM)*, vol. 1, 2020, pp. 2342–2348.

[4] "Electrical and Electronics Technical Team Roadmap," https://www.energy.gov/sites/prod/files/2017/11/f39/EETT%20Roadmap%2010-27-17.pdf.

[5] I. Husain, B. Ozpineci, M. S. Islam, E. Gurpinar, G.-J. Su, W. Yu, S. Chowdhury, L. Xue, D. Rahman, and R. Sahu, "Electric drive technology trends, challenges, and opportunities for future electric vehicles," *Proceedings of the IEEE*, vol. 109, no. 6, pp. 1039–1059, 2021.

[6] S. Huang, A. Aggarwal, E. G. Strangas, K. Li, F. Niu, and X. Huang, "Robust stator winding fault detection in pmsms with respect to current controller bandwidth," *IEEE Transactions on Power Electronics*, vol. 36, no. 5, pp. 5032–5042, 2021.

[7] A. Aggarwal, E. G. Strangas, and J. Agapiou, "Analysis of unbalanced magnetic pull in pmsm due to static eccentricity," in *2019 IEEE Energy Conversion Congress and Exposition (ECCE)*, 2019, pp. 4507–4514.

[8] A. Aggarwal and E. G. Strangas, "Review of detection methods of static eccentricity for interior permanent magnet synchronous machine," *Energies*, vol. 12, no. 21, p. 4105, 2019.

[9] G.-J. Li, Z.-Q. Zhu, M. P. Foster, D. A. Stone, and H.-L. Zhan, "Modular permanent-magnet machines with alternate teeth having tooth tips," *IEEE Transactions on Industrial Electronics*, vol. 62, no. 10, pp. 6120–6130, 2015.

[10] R. Wrobel and B. Mecrow, "A comprehensive review of additive manufacturing in construction of electrical machines," *IEEE Transactions on Energy Conversion*, vol. 35, no. 2, pp. 1054–1064, 2020.

[11] A. Aggarwal, M. Matthew, E. G. Strangas, and A. Agapiou, "Analysis of modular stator pmsm manufactured using oriented steel," in *Energies MDPI AG*, vol. 14, no. 20, 2021, p. 6583.

[12] T. Pham, P. Kwon, and S. Foster, "Additive manufacturing and topology optimization of magnetic materials for electrical machines—a review," *Energies*, vol. 14, no. 2, 2021. [Online]. Available: https://www.mdpi.com/1996-1073/14/2/283

[13] E. Périgo, J. Jacimovic, F. García Ferré, and L. Scherf, "Additive manufacturing of magnetic materials," *Additive Manufacturing*, vol. 30, p. 100870, 2019. [Online]. Available: https://www.sciencedirect.com/science/article/pii/S2214860419305056

[14] Z.-Y. Zhang, K. J. Jhong, C.-W. Cheng, P.-W. Huang, M.-C. Tsai, and W.-H. Lee, "Metal 3d printing of synchronous reluctance motor," in *2016 IEEE International Conference on Industrial Technology (ICIT)*, 2016, pp. 1125–1128.

[15] Z.-Y. Zhang, M.-C. Tsai, P.-W. Huang, C.-W. Cheng, and J.-M. Huang, "Characteristic comparison of transversally laminated anisotropic synchronous reluctance motor fabrication based on 2d lamination and 3d printing," in *2015 18th International Conference on Electrical Machines and Systems (ICEMS)*, 2015, pp. 894–897.

[16] G.-M. Tseng, K.-J. Jhong, M.-C. Tsai, P.-W. Huang, and W.-H. Lee, "Application of additive manufacturing for low torque ripple of 6/4 switched reluctance motor," in *2016 19th International Conference on Electrical Machines and Systems (ICEMS)*, 2016, pp. 1–4.

[17] S. Urbanek, B. Ponick, A. Taube, K.-P. Hoyer, M. Schaper, S. Lammers, T. Lieneke, and D. Zimmer, "Additive manufacturing of a soft magnetic rotor active part and shaft for a permanent magnet synchronous machine," in *2018 IEEE Transportation Electrification Conference and Expo (ITEC)*, 2018, pp. 668–674.

[18] S. Urbanek, P. Frey, S. Magerkohl, D. Zimmer, L. Tasche, M. Schaper, and B. Ponick, "Design and experimental investigation of an additively manufactured pmsm rotor," in *2021 IEEE International Electric Machines Drives Conference (IEMDC)*, 2021, pp. 1–6.

[19] L. Gargalis, V. Madonna, P. Giangrande, R. Rocca, M. Hardy, I. Ashcroft, M. Galea, and R. Hague, "Additive manufacturing and testing of a soft magnetic rotor for a switched reluctance motor," *IEEE Access*, vol. 8, pp. 206 982–206 991, 2020.

[20] T. Huguet, J. Šafka, C. Nadal, F. Véle, M. Ackermann, and C. Henaux, "Perfomances evaluation of a 3d printed rotor for a synchronous reluctance machine," in *2021 IEEE International Workshop of Electronics, Control, Measurement, Signals and their application to Mechatronics (ECMSM)*, 2021, pp. 1–8.

[21] D. Goll, D. Schuller, G. Martinek, T. Kunert, J. Schurr, C. Sinz, T. Schubert, T. Bernthaler, H. Riegel, and G. Schneider, "Additive manufacturing of soft magnetic materials and components," *Additive Manufacturing*, vol. 27, pp. 428–439, 2019. [Online]. Available: https://www.sciencedirect.com/science/article/pii/S2214860418310467

[22] H. Tiismus, A. Kallaste, A. Belahcen, M. Tarraste, T. Vaimann, A. Rassõlkin, B. Asad, and P. Shams Ghahfarokhi, "AC Magnetic Loss Reduction of SLM Processed Fe-Si for Additive Manufacturing of Electrical Machines," *Energies*, vol. 14, no. 5, 2021. [Online]. Available: https://www.mdpi.com/1996-1073/14/5/1241

[23] T. Q. Pham, H. Suen, P. Kwon, and S. N. Foster, "Reduction in hysteresis loss of binder jet printed iron silicon," in *2020 International Conference on Electrical Machines (ICEM)*, vol. 1, 2020, pp. 1669–1675.

[24] T. Do, C. S. Shin, D. Stetsko, G. VanConant, A. Vartanian, S. Pei, and P. Kwon, "Improving Structural Integrity with Boron-based Additives for 3D Printed 420 Stainless Steel, journal = Procedia Manufacturing," vol. 1, pp. 263–272, 2015, 43rd North American Manufacturing Research Conference, NAMRC 43, 8-12 June 2015, UNC Charlotte, North Carolina, United States. [Online]. Available: https://www.sciencedirect.com/science/article/pii/S2351978915010197

[25] Y. Wan and W. Chen, "Effect of boron content on the microstructure and magnetic properties of non-oriented electrical steels," *Journal Wuhan University of Technology, Materials Science Edition*, vol. 30, no. 3, pp. 574–579, 2015.

[26] T. Stovall, F. de Larrard, and M. Buil, "Linear packing density model of grain mixtures," *Powder Technology*, vol. 48, no. 1, pp. 1–12, 1986. [Online]. Available: https://www.sciencedirect.com/science/article/pii/0032591086800584

[27] "Standard Test Method for Direct Current Magnetic Properties of Low Coercivity Magnetic Materials Using Hysteresigraphs," *ASTM International Std. A773/A773M*, 2014.

[28] "Standard Test Method for Alternating-Current Magnetic Properties of Toroidal Core Specimens Using the Voltmeter-Ammeter-Wattmeter Method," *ASTM International Std. A927/A927M*, 2018.

[29] Altair, *Altair FluxMotor (Version 2019.1.1)*, Altair Engineering Inc., 2019. [Online]. Available: https://www.altair.com/fluxmotor/

[30] JMAG, *JMAG-Designer (Version 20.2)*, JSOL Corporation, 2021. [Online]. Available: https://www.jmag-international.com/products/jmag-designer/index_v202/

[31] "Iron Loss Analysis of an IPM Motor," *JMAG Application Note JAC069*, 2009. [Online]. Available: https://www.jmag-international.com/catalog/69_ipmmotor_ironloss/

## VII. Biographies

**Bhuvan Khoshoo** (Student Member, IEEE) received the B.Tech. degree in electrical engineering from National Institute of Technology, Raipur, India, in 2012. He is currently working toward the Ph.D. degree in electrical and computer engineering with Electric Machines and Power Electronics Research (EMPowER) Laboratory at Michigan State University, East Lansing, MI, USA. From July 2012 to May 2018, he was with Schneider Electric, India as an Electromechanical Engineer. His research interests include design, optimization, and control of electric machines and drives.

**Khan Jazib Islam** received the B.Tech. degree in electrical engineering from Zakir Husain College of Engineering and Technology, Aligarh Muslim University, Aligarh, India, in 2017. He is currently working towards the Master's degree in electrical and computer engineering with the Electric Machines and Power Electronics Research (EMPowER) Laboratory at Michigan State University, East Lansing, MI, USA. His research interests include design, optimization, and control of electric machines and drives.

**Hawke Suen** received the B.S. degree in mechanical engineering from Michigan State University, East Lansing, MI, USA, in 2017. He is currently working toward the Ph.D. degree in metal additive manufacturing with the Department of Mechanical Engineering, Michigan State University, East Lansing, MI, USA. His research interests include process optimization on manufacturing metal materials in additive manufacturing.

**Patrick Kwon** received the B.S. degree in mechanical engineering from the University of Michigan, Ann Arbor, Ann Arbor, MI, USA, in 1983, the M.S. degree in mechanical engineering from the Massachusetts Institute of Technology, Cambridge, MA, USA, in 1985, and the Ph.D. degree in mechanical engineering from the University of California, Berkeley, Berkeley, CA, USA, in 1994.

He was with GM briefly and Materials Integrity Solution as a Research Engineer. He started his academic career as an Assistant Professor with the Department of Materials Science and Mechanics, Michigan State University (MSU), East Lansing, MI, USA, in 1996 and moved over to Department of Mechanical Engineering in 2000. He was promoted to Professor with the Department of Mechanical Engineering, MSU in 2002. He was a Visiting Professor with the Ulsan National Institute of Science and Technology (UNIST), Ulsan, South Korea, in 2007. He was the Director of NSF's I/UCRCenter for Advanced Cutting Tool Technology from 2008 to 2017. His research areas include various aspects of machining and powder processing including metal additive manufacturing.

Dr. Kwon was an Associate Editor for the ASME Journal of Manufacturing Science and Engineering between 2009 and 2015 and has been an Associate Editor for the International Journal of Precision Engineering and Manufacturing since 2012. He has been an Associate Chair for Graduate Studies, Department of Mechanical Engineering since 2017.

**Jorge Peña Lozano** Jorge Peña is an undergaduate student, pursuing a major in electrical engineering from Michigan State University, East Lansing, MI, USA. He is currently working as a research assistant with Electric Machines and Power Electronics Research (EMPowER) Laboratory at Michigan State University. His research interests include power electronics, energy conversion analysis, biomedicine and sustainability.

**Shanelle N. Foster** (Senior Member, IEEE) received the B.S., M.S., and Ph.D. degrees in electrical engineering from Michigan State University, East Lansing, MI, USA, in 1996, 1998, and 2013 respectively. She is currently an Assistant Professor with the Department of Electrical and Computer Engineering, Michigan State University. Her research interests include analysis, control, reliability, and manufacturability of rotating, and linear electrical machines and drives.